Carbohydrate Polymers 106 (2014) 190–199

Contents lists available at ScienceDirect

Carbohydrate Polymers

journal homepage: www.elsevier.com/locate/carbpol

Properties and characterization of bionanocomposite films prepared with various biopolymers and ZnO nanoparticles

Paulraj Kanmani, Jong-Whan Rhim *

Department of Food Engineering and Bionanocomposite Research Institute, Mokpo National University, 61 Dorimri, Chungkyemyon, Muangun, 534-729, Jeonnam, Republic of Korea

ARTICLE INFO

Article history:
Received 24 November 2013
Received in revised form 2 February 2014
Accepted 3 February 2014
Available online 10 February 2014

Keywords:
Biopolymers
ZnO nanoparticles
Nanocomposite
Antimicrobial activity
Active food packaging

ABSTRACT

This study was aimed to develop biopolymer based antimicrobial films for active food packaging and to reduce environmental pollution caused by accumulation of synthetic packaging. The ZnO NPs were incorporated as antimicrobials into different biopolymers such as agar, carrageenan and CMC. Solvent casting method was performed to prepare active nanocomposite films. Methods such as FE-SEM, FT-IR and XRD were used to characterize resulting films. Physical, mechanical, thermal and antimicrobial properties were also examined. Remarkable surface morphological differences were observed between control and nanocomposite films. The crystallinity of ZnO was confirmed by XRD analysis. The addition of ZnO NPs increased color, UV barrier, moisture content, hydrophobicity, elongation and thermal stability of the films, while decreased WVP, tensile strength and elastic modulus. ZnO NPs impregnated films inhibited growth of *L. monocytogenes* and *E. coli*. So these newly prepared nanocomposite films can be used as active packaging film to extend shelf-life of food.

1. Introduction

Recently, tremendous research works on exploring natural biopolymers for the development of environment friendly packaging materials as alternatives of non-biodegradable petroleum-based synthetic plastic materials (Shojaee-Aliabadi et al., 2013). This is mainly due to their enhanced biodegradability, biocompatibility, edibility and sustainability (Salmieri & Lacroix, 2006). Polysaccharides, proteins, and lipid materials from plant and animal origin are usually used for this purpose. Among those biopolymer materials, polysaccharide-based biopolymers are particularly attractive due to their good film forming property, moderate mechanical strength and gas barrier properties with unique colloidal nature. Various polysaccharides such as chitosan, agar, carrageenan, cellulose and its derivatives, alginate, pectin, starch, pullulan, etc., have been tested to make packaging films (Rhim et al., 2006; Rhim & Ng, 2007; Rhim, 2011; Nafchi et al., 2012; Espitia et al., 2013; Kanmani & Lim, 2013).

However, biopolymer-based packaging materials have not been widely used in the packaging industry, mainly because of their poor mechanical, barrier, and processing properties as well as higher production cost compared with commodity plastic films (Tunç & Duman, 2011). One of the methods to overcome such shortcomings of biopolymer-based packaging materials is to make hybrid with other materials. Recent research works have shown that homogeneous blending of biopolymer with various types of nano-sized filler materials resulted in the improvement of the physical, mechanical and gas barrier properties of the films (Kurian et al., 2006; Yu et al., 2009; Yoksan & Chirachanchai, 2010). These are mainly due to the strong interfacial interaction between the filler (with large specific surface area) and polymer matrix and the formation of tortuous pathway of gas diffusion caused by the impervious nanofillers. In addition, some nanofillers such as organically modified nanoclays with quaternary ammonium salt (Hong & Rhim, 2008) and nano-sized metals or metallic oxides are known to have strong antimicrobial activity against diverse group of gram-positive and gram-negative bacterial and fungal pathogens. Therefore, various types of such nanostructured particles have been used to prepare antimicrobial packaging materials (Llorens et al., 2012; Kanmani & Rhim, 2014).

As one of such metallic oxide nanoparticles, zinc oxide nanoparticles (ZnO NPs) are attractive, especially in food packaging industry because of their potent and broad spectrum of antimicrobial property (Li et al., 2009; Espitia et al., 2013). The ZnO NPs are found to have large surface to volume ratio, chemically alterable physical property, increased surface reactivity, unique thermal, mechanical and electrical properties (Sharon et al., 2010).

* Corresponding author. Tel.: +82 61 450 2423; fax: +82 61 454 1521.
E-mail addresses: jwrhim@mokpo.ac.kr, jwrhim@hanmail.net (J.-W. Rhim).

http://dx.doi.org/10.1016/j.carbpol.2014.02.007
0144-8617/

In addition, they are heat stable and generally recorded as safe (GRAS) substance approved by Food and Drug Administration (FDA, 2011). The ZnO nanoparticles have been incorporated into several polymer films to produce antimicrobial nanocomposite packaging films (Yu et al., 2009; Espitia et al., 2013). The antimicrobial nanocomposite is a type of active food packaging system which can be interacted with packaged product to reduce the growth of microorganisms present on the surface of food stuffs (Soares et al., 2009).

Variety of polysaccharides has been used as a carrier of active antimicrobial agents such as metal or metallic oxide nanoparticles. Some of the polysaccharides tested for this purpose include agar, carrageenan, and carboxymethyl cellulose (CMC) since they are biodegradable, biocompatible, annually-renewable, and abundantly available with good film forming property (Yu et al., 2009; Almasi et al., 2010; Shojaee-Aliabadi et al., 2013; Gimenez, Lopez de Lacey, Perez-Santí, Lopez-Caballero, & Montero, 2013; Rhim et al., 2013). However, antimicrobial activity and other film properties of those polysaccharide-based nanocomposite films are expected to depend on the type of polysaccharide used.

Therefore the main objective of the present study was to develop active bio-based nanocomposite films by mixing of various biopolymers such as agar, carrageenan, and CMC with ZnO NPs in order to test the effect of type of polysaccharide polymer matrix on the film properties and antimicrobial activity. The films were characterized by SEM, XRD, FT-IR, and TGA analysis. The antimicrobial activity of the films was also tested against two selected food borne pathogens.

2. Materials and methods

2.1. Materials and microbial strains

Agar, κ-carrageenan and carboxymethyl cellulose (CMC) were obtained from Fine Agar Agar Co., Ltd. (Damyang, Jeonnam, Korea), Hankook Carragen (Whasoon, Jeonnam, Korea), and Hercules Chemicals Co., Ltd. (Jianmen, China), respectively. Zinc acetate, sodium hydroxide and glycerol were procured from Daejung Chemicals & Metals Co., Ltd. (Siheung, Gyonggido, Korea). Microbiological media such as tryptic soy broth (TSB), brain heart infusion broth (BHI), and agar powder were purchased from Duksan Pure Chemicals Co., Ltd (Ansan, Gyeonggi-do, Korea). Pathogenic microorganisms such as *Escherichia coli* O157:H7 ATCC 43895 and *Listeria monocytogenes* ATCC 15313 were procured from Korean collection for type cultures (KCTC, Seoul, Korea). Both of these strains were grown in TSA and BHI agar medium and stored at 4 °C for further experiment. All the solutions were prepared using ultra-filtered high purity deionized water.

2.2. Preparation of films

Agar, carrageenan, and CMC films and their ZnO nanocomposite films were prepared by the solution casting method (Rhim et al., 2013). To produce zinc oxide nanoparticles (ZnO NPs), zinc acetate (0.1 M) was dissolved in 150 mL of hot water and mixed completely by stirring at 80 °C for 20 min using a magnetic stirrer. Then 1.6 mL of NaOH (2.5 M) solution was added drop wise into the zinc acetate solution and continued stirring at the same temperature for 1 h. White color precipitation was formed which indicates formation of ZnO NPs. Then 3 g of biopolymers, agar, carrageenan, and CMC, were added slowly into the nanoparticles solution (150 mL) with stirring until they dissolved completely, and glycerol (0.9 g) was added into the polymer/nanoparticles solutions with stirring at 80 °C for 20 min. The complete solubilized film forming solutions were cast evenly onto a leveled Teflon film (Cole-Parmer Instrument Co., Chicago, IL, USA) coated glass plate (24 × 30 cm), and allowed to dry at room temperature (23–25 °C) for 2 days. The completely dried all nanocomposite films were peeled off from the glass plate and preconditioned at 25 °C and 50% RH for 48 h in a constant temperature humidity chamber to normalize the moisture content of the films prior to further characterizations. The control biopolymer films were prepared with the same method without addition of ZnO NPs.

2.3. Morphological observation

Scanning electron microscopy (SEM) analysis was performed to observe the microstructure of the film samples. Small piece of film sample was mounted on a SEM specimen holder and analyzed using a field emission scanning electron microscopy (FE-SEM, S-4800, Hitachi Co., Ltd., Matsuda, Japan) with an accelerating voltage of 5.0 kV.

2.4. FT-IR and XRD analysis

Fourier transform infrared (FT-IR) spectrum of the film samples was measured using a FT-IR spectroscopy (TENSOR 37 spectrophotometer with OPUS 6.0 software, Billerica, MA, USA) operated at a resolution of 4 cm^{-1}. Film samples were cut into rectangular shape (5 × 5 cm) and directly placed on the ray exposing stage. The spectrum was recorded at wave number of 500–4000 cm^{-1}.

X-ray diffraction (XRD) pattern of the film samples was analyzed by X-ray diffractometer (PAN analytical X-pert pro MRD diffractometer, Amsterdam, Netherlands). Samples were prepared by placing rectangular shape of each film (2.5 × 2.5 cm) on a glass slide and the spectra were recorded using Cu-Kα radiation and a nickel monochromator filtering wave at 40 kV and 30 mA with scanning at 2θ = 10–50°.

2.5. Measurement of surface color

Surface color of the film samples was measured using a Chroma meter (Minolta, CR-200, Tokyo, Japan) with a white color plate (L^* = 97.75, a^* = −0.49, and b^* = 1.96) as a standard background for color measurement. The CIE color values (L^*, a^* and b^*) were determined by average of five readings from each film sample. Total color difference (ΔE) was calculated as follows:

$$\Delta E = [(\Delta L*)^2 + (\Delta a*)^2 + (\Delta b*)^2]^{0.5} \quad (1)$$

where ΔL^*, Δa^*, and Δb^* are the difference between the color of standard plate and film samples.

2.6. UV and transparency

Optical property of the film samples was determined by measuring light absorption spectra and transparency of the film samples. Each film sample was cut into a rectangular piece and directly mounted between two spectrophotometer magnetic cells. Both the absorbance and percent transmittance spectra were measured using a UV–vis spectrophotometer (Model 8451A, Hewlett-Packard Co., Santa Alara, CA, USA) in the wavelength of 200–700 nm. Transparency of the films was tested by measuring percent transmittance at both UV ($T_{280\,nm}$) and visible ($T_{660\,nm}$) ranges at 280 and 660 nm, respectively.

2.7. Water vapor permeability (WVP)

The water vapor permeability of the film samples was determined gravimetrically according to the method of ASTM E96-95 with slight modification (Gennadios et al., 1994). Rectangular film samples (7.5 × 7.5 cm) were mounted horizontally on the

WVP measuring cups which were made of flaxy glass, poly (methylmethacrylate) with inside depth and diameter of 2.5 and 6.8 cm, respectively, filled with distilled water up to 1 cm underneath the film. The cups were placed in an environmental chamber controlled at 25 °C and 50% RH with air current movement at 198 m/min. The cup was weighed every hour for a period of 8 h. Water vapor transmission rate (WVTR) was determined from the slopes of the steady state portion of weight loss of the cup versus time curve. Then the WVP of the films in $g \cdot m/m^2 \cdot s \cdot Pa$ was calculated as follows:

$$WVP = \frac{(WVTR \times L)}{\Delta p} \quad (2)$$

where WVTR was the measured water vapor transmission rate ($g/m^2 \cdot s$) through a film, L was the mean film thickness (m), and Δp was the partial water vapor pressure difference (Pa) across the two sides of the film.

2.8. Water contact angle (WCA)

The surface hydrophobic or hydrophilic character of the film samples was determined using the WCA analyzer (model Phoenix 150, Surface Electro Optics Co., Ltd., Kunpo, Korea). Each film sample was cut into rectangular piece (3 × 10 cm) and directly placed on the horizontal movable stage (Black Teflon coated steel, 7 × 11 cm) fixed with contact angle analyzer. 10 μL of water was dropped on surface of the film using a micro syringe and measured the contact angle on both sides of the water drop to assume symmetry and horizontal level (Rhim et al., 2006).

2.9. Moisture content (MC)

The MC of the film samples was determined according to the method of Soradech, Nunthanid, Limmatvapirat, and Luangtana-anan (2012). To this analysis, each film sample was cut into 3 × 3 cm and dried at 100 °C for 24 h using a hot air oven. Before and after drying, the weight loss of each film sample was measured as water content and expressed as percent MC based on the initial weight of film.

2.10. Thickness and mechanical properties of the films

Thickness of the film samples was measured using a hand-held micrometer (Dial Thickness Gauge 7301, Mitutoyo Corporation, Kanagawa, Japan) with an accuracy of 0.01 mm. Six random measurements were taken from each film sample and the average values were used as the film thickness.

The mechanical properties of the film samples were measured according to the standard test method of ASTMD-882-88. The mechanical properties such as tensile strength (MPa), elongation at break (%), and elastic modulus (MPa) were measured using Instron Universal Testing Machine (Model 5565, Instron Engineering Corporation, Canton, Mass, U.S.A.). Each film sample was cut into rectangular strip (2.54 × 15 cm) and stretched with an initial grip separation of 50 mm and crosshead speed at 50 mm/min, respectively. Ten measurements were carried out for each film sample and the average values were presented.

2.11. Thermal stability

Thermal stability of the film samples was tested using a thermogravimetric analyzer (TGA; Hi-Res TGA 2950 thermo gravimetric analyzer, TA Instrument). Each film sample (about 5 mg) was taken in standard aluminum cup and scanned at heating rate of 10 °C/min with temperature ranged from 30–600 °C under a nitrogen flow of 50 cm^3/min. Derivative form of TGA (DTGA) was obtained by differentials of TGA values and calculated as follows (Rhim et al., 2013):

$$DTGA = \frac{(w_{t+\Delta t} - w_{t-\Delta t})}{2\Delta t} \quad (3)$$

where $w_{t+\Delta t}$ and $w_{t-\Delta t}$ are residual weight of sample at time $t + \Delta t$ and $t - \Delta t$, respectively, and Δt is the time interval for reading residual sample weight.

2.12. Antimicrobial activity

The antimicrobial activity of the film samples was evaluated against food borne pathogens such as *E. coli* and *L. monocytogenes* using a colony count method. All the strains were aseptically inoculated in TSB and BHI broth and subsequently incubated at 37 °C for 16 h. Each cultured broth (20 mL) was centrifuged at 5000 rpm for 10 min. The cell pellet was suspended with 100 mL of sterile TSB and BHI broth and diluted by 1/10 volume with sterile water. 50 mL of diluted broth ($\sim 10^6$ CFU mL^{-1}) was taken into 100 mL of conical flask containing film sample (5 × 5 cm) and subsequently incubated at 37 °C for 12 h under mild shaking. The same diluted broth without film sample was used as the control. At every two hour interval, the cell viability of each pathogen was calculated by counting bacterial colonies on the plates.

2.13. Statistical analysis

Measurements of each property were triplicated for color, TS, E, EM, WVP, and WCA as well as the antimicrobial test with individually prepared films as the triplicate experimental units. The software package SPSS version 12.0 (SPSS Inc., Chicago, IL, USA) was used for statistical analysis. One-way analysis of variance (ANOVA) was performed and the significant differences among the values of film samples were determined using Tukey's test with significant level of $p = 0.05$.

3. Results and discussion

3.1. Surface morphology

The surface morphology of the neat agar, carrageenan, CMC, and their nanocomposite films were examined by SEM microcopy. As can be seen in Fig. 1, smooth and compact surface morphologies were observed for neat films, while nanocomposite films showed rough surface structures with evenly distributed ZnO NPs. SEM results showed that the ZnO NPs were homogenously distributed through the whole film surfaces. They also exhibited the presence of ZnO NPs with different shapes and some aggregation of ZnO NPs in the films surfaces. Li and Haneda (2003) observed four different shapes of ZnO such as rod, spherical shaped, intertwined needle and ellipsoidal aggregates. Similar surface morphologies were obtained with addition of ZnO NPs into some other polymeric films such as GPS/CMC (Yu et al., 2009), methyl cellulose (Espitia et al., 2013), PUA (Kim et al., 2012), and PP film (Paisoonsin et al., 2013).

3.2. FT-IR and XRD analysis

FT-IR analysis was performed to examine the interactions between polymer and ZnO NPs. Fig. 2 shows FT-IR spectra of the neat agar, carrageenan, CMC, and their nanocomposite films respectively. The spectra of all neat films displayed characteristic peaks in the range of 3360 to 671 cm^{-1}. The characteristic broad absorption band at about 3360–3333 cm^{-1} was attributed to the stretching of hydroxyl (O—H) groups (Wu et al., 2009). The intense peak appeared at 2928–2937 cm^{-1} was due to the stretching of

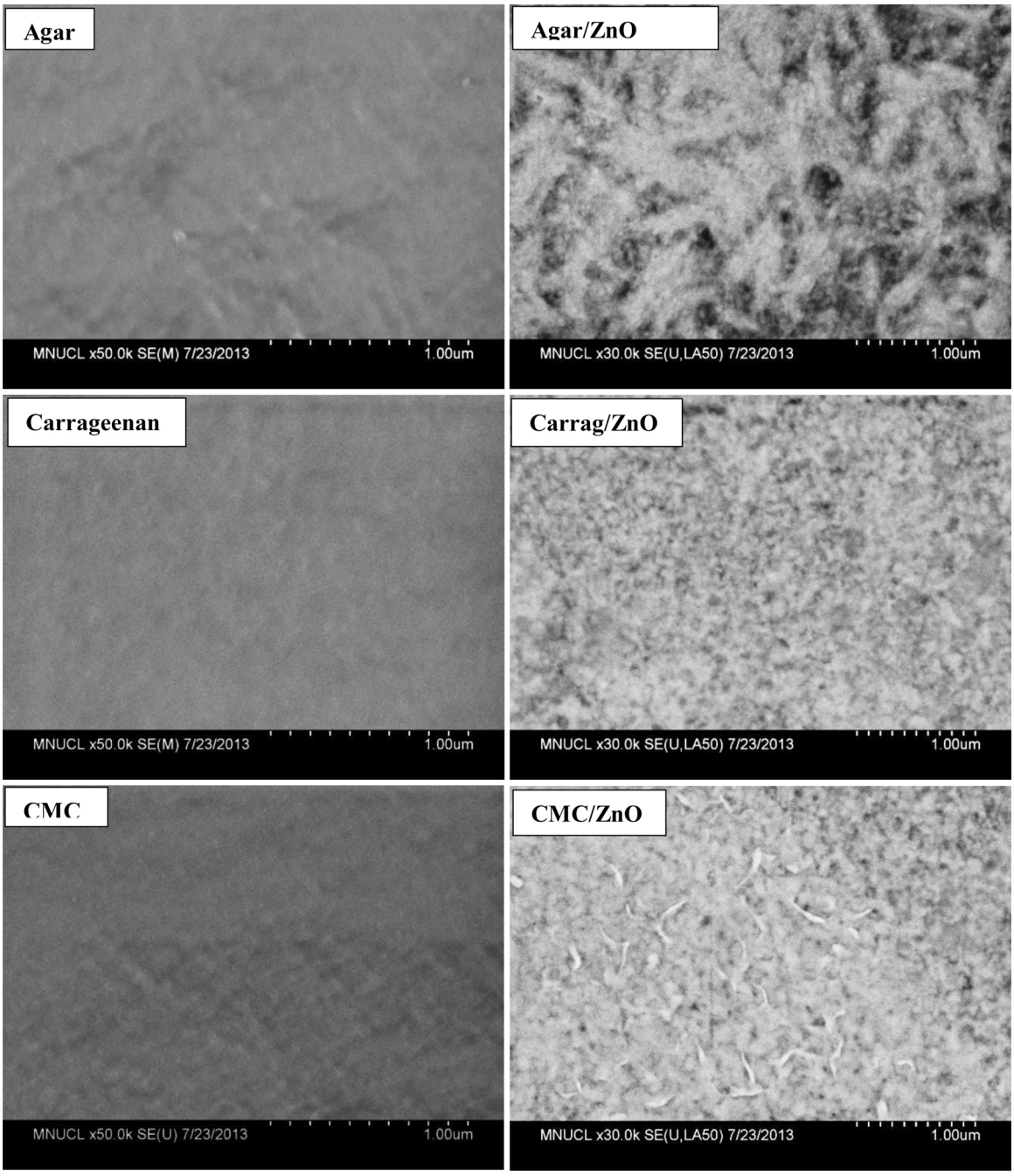

Fig. 1. SEM micrograph of the neat agar, carrageenan, CMC, and their nanocomposite films. White color indicates the uniform distribution of ZnO NPs.

C—H which was associated with the ring of methane hydrogen atoms (Yu et al., 2009). The peak at 1640 cm^{-1} in the FT-IR spectra of agar was attributed to the stretching vibration of the conjugated peptide bond formation by amine (NH) and acetone groups (Wu et al., 2009). The CMC film exhibited two peaks at 1416 and 1590 cm^{-1} which indicated symmetrical and asymmetrical stretching vibrations of the carboxylate group (Rosca et al., 2005). The appeared absorption bands at 1372 cm^{-1} and 1220 cm^{-1} in the agar and carrageenan films were assigned to ester sulfate (Volery et al., 2004). The characteristic absorption peaks at 1074, 1040 and 931 cm^{-1} indicated C—O stretching group of 3,6-anhydro-galactose. Likewise, C—O stretching peaks were exhibited by CMC at 1000–1200 cm^{-1}. The peak at 886 cm^{-1} in the agar film was related to the C—H stretching residual carbon of β-galactose (Wu et al., 2009). As can be seen in Fig. 2, similar kinds of peaks with high intensity were observed in the FT-IR spectra of the nanocomposite films. However, some of the peaks were shifted to higher and lower wave number with addition of ZnO NPs. For example in the FT-IR of agar based films, peaks at 3333, 2928, 1640, and 1040 cm^{-1} were shifted to 3340, 2935, 1569, and 1049 cm^{-1}, respectively. The shifting of absorption peaks indicated that certain interactions between ZnO NPs and biopolymer matrix were formed (Anitha et al., 2012). Two more extra peaks were also observed in the FI-IR spectra of the nanocomposite films, probably due to the vibration of ZnO.

X-ray diffraction (XRD) patterns of the neat agar, carrageenan, CMC, and their nanocomposite films were shown in Fig. 3. While the neat films didn't show diffraction peaks, the nanocomposite films exhibited characteristic diffraction peaks at 2θ of 32.0, 34.4,

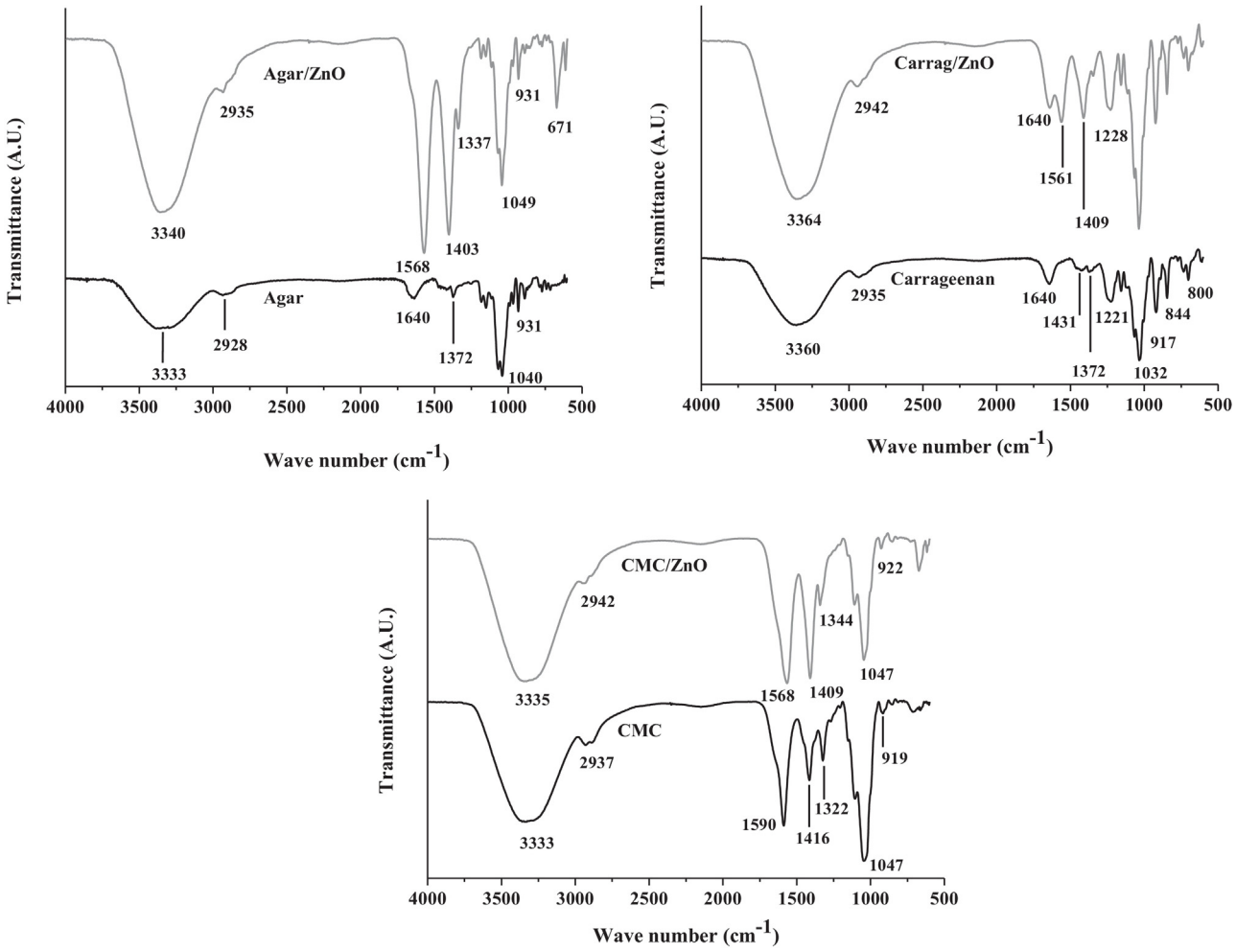

Fig. 2. Fourier transform infra-red (FT-IR) spectra of the neat agar, carrageenan, CMC and their ZnO nanocomposite films.

36.6, 48.5 and 56.5, which corresponds to (100), (002), (101), (102), and (110) planes of zinc oxide, respectively. These diffraction peaks confirmed the presence of crystal zinc oxide (Tankhiwale & Bajpai, 2012). Similar results were observed with other ZnO incorporated nanocomposites such as CA/ZnO (Anitha et al., 2012) and CMC/ZnO (Yu et al., 2009).

3.3. Surface color

Surface color of food packaging films is an important parameter since it influences the general appearance and consumer acceptance (Srinivasa et al., 2003; Tharanathan, 2003). The color properties of the neat agar, carrageenan, CMC films and their nanocomposite films are summarized in Table 1. The incorporation of ZnO NPs affected color properties of all of the biopolymer films. The L^*-values decreased slightly and a^*-values decreased significantly, while b^*-values increased significantly by the addition of ZnO NPs into the agar, carrageenan, and CMC films. This result indicates the lightness of the films decreased with increase in the greenness and yellowness of the films after formation of nanocomposite with the ZnO NPs. The total color difference (ΔE) of the nanocomposite films increased compared with those of neat biopolymer films. The ΔE of the neat agar, carrageenan and CMC films were 2.15 ± 0.23, 1.35 ± 0.4, and 1.13 ± 0.55, respectively, and they increased to 4.22 ± 0.09, 1.88 ± 0.22, and 1.34 ± 0.22 after blending with ZnO NPs. The ΔE of agar-based films increased more than those of carrageenan and CMC-based films. These results are in good agreement with those of Nafchi et al. (2012) who found that the sago starch/ZnO films had significantly lower L^*-value with higher a^*- and b^*-values compared with those of neat sago starch film.

3.4. Optical properties

The optical properties of the biopolymer films and their nanocomposite films were studied by measuring absorbance using a UV–vis spectrophotometer and the results were shown in Fig. 4. No absorption peaks were observed for the control biopolymer films in the range of 200–700 nm. However, films blended with ZnO NPs showed clear absorption peak at 360–380 nm. Agar/ZnO nanocomposite film exhibited higher absorption peak compared with those of carrageenan/ZnO and CMC/ZnO nanocomposites films. The agar/ZnO and carrageenan/ZnO nanocomposite films showed peaks at 360–370 nm while just extended peak (380) nm was observed for CMC/ZnO nanocomposite film. Similar result was observed with CMC/ZnO nanocomposite films (Yu et al., 2009). Kim et al. (2012) also found that the ZnO NPs blended PUA film showed absorption peak at 360–380 nm. They also found that the absorption peak increased as the concentration of ZnO NPs increased from 1 % to 10 %.

The percent transmittance of light at UV and visible regions was measured and the results are shown in Table 1. The neat agar, carrageenan and CMC films were transparent with high transmittance values at both UV and visible region. Transmittance of the

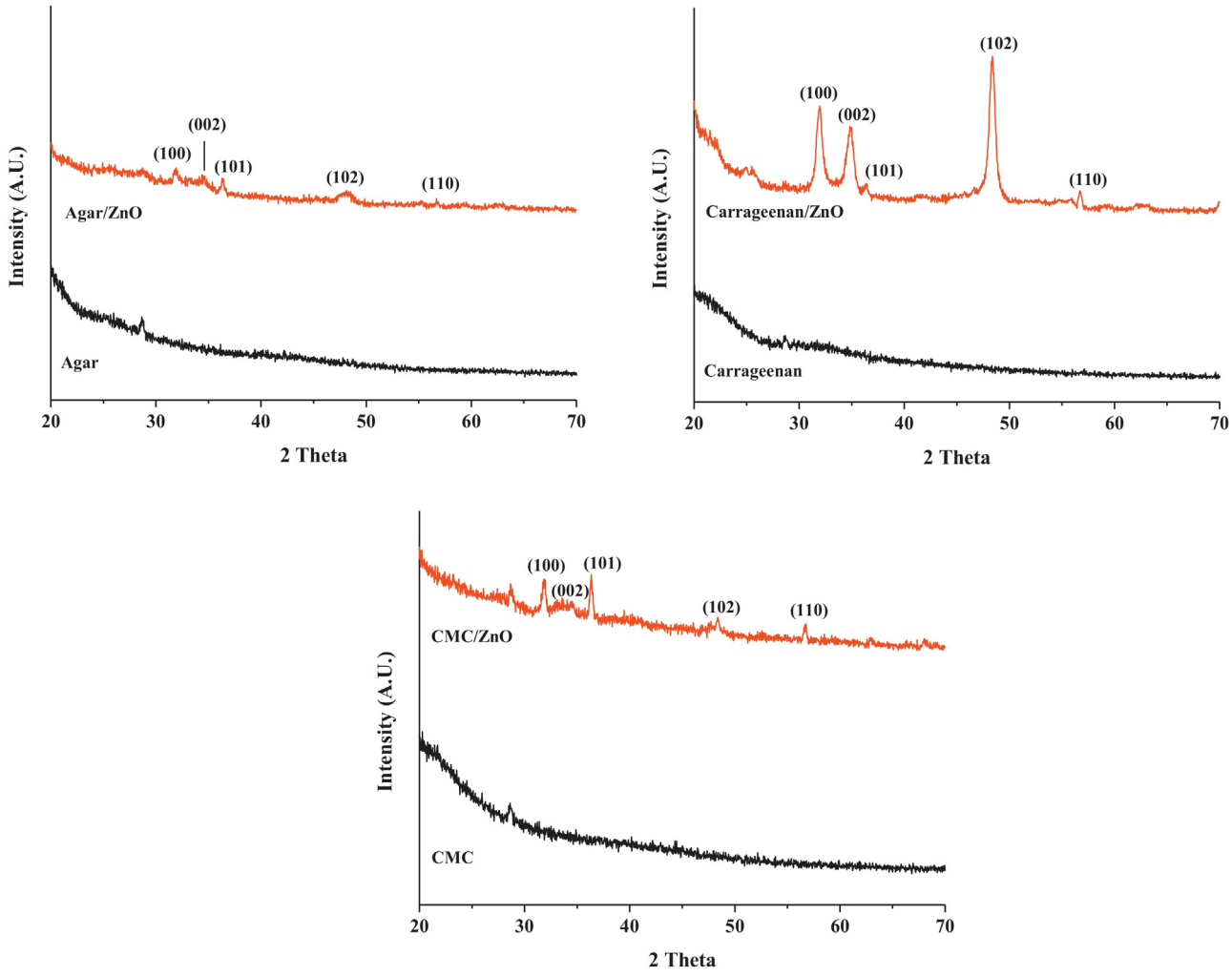

Fig. 3. X-ray diffraction (XRD) patterns of the various nanocomposite films.

biopolymer films was also greatly influenced by the formation of nanocomposite with ZnO. Generally, both transmittance values of all of the biopolymer films decreased significantly. However, it is interesting to note that the decrease in the transmittance in the visible range ($T_{660\,nm}$) of the biopolymer films except CMC film was slight, but the decrease in the transmittance in the UV range ($T_{280\,nm}$) was profound. Among the nanocomposite films tested, CMC/ZnO NPs exhibited lower light transmission values than the other nanocomposite films. As shown in Table 1, more than 93% and 90% of the UV light were absorbed by agar/ZnO NPs and CMC/ZnO NPs nanocomposite films, which indicated that the ZnO NPs in the film matrices prevented the passage of UV light. Similar results have been observed for other nanocomposite films such as sago starch/ZnO (Nafchi et al., 2012), PUA/ZnO (Kim et al., 2012), and CMC/ZnO (Yu et al., 2009). The nanocomposite films with strong UV prevention capacity without sacrificing transparency are expected to be used as a food packaging needed for UV screening.

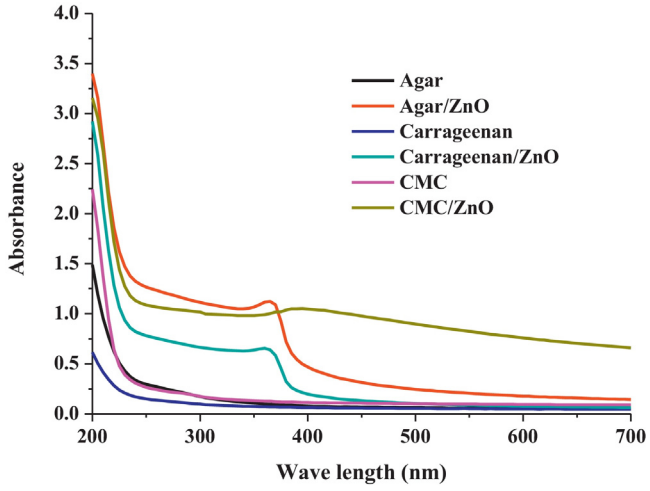

Fig. 4. UV–vis absorption spectra of the neat agar, carrageenan, CMC and their ZnO nanocomposite films.

3.5. Moisture content (MC) and hydrophobicity of the films

Table 2 shows moisture content (MC) of the neat agar, carrageenan, CMC films and their nanocomposite films. Compared with the control films, the nanocomposite films exhibited slightly higher MC, however, they were not significantly different ($p > 0.05$). Among the films tested, carrageenan based films retained slightly lower MC than the other films.

Surface wettability and hydrophobicity of the neat and nanocomposite films were tested by measuring the water contact angle (WCA) (Table 2). The WCA (degree) of the neat agar, carrageenan and CMC were 66.5 ± 1.4, 61.5 ± 3.0, and 31.6 ± 2.0, respectively. The WCA values of the films were significantly ($p < 0.05$) increased up to

Table 1
Color and percent transmittance values of various biopolymer based nanocomposite films.

Films	L	a	b	ΔE	$T_{280\,nm}$ (%)	$T_{660\,nm}$ (%)
Agar	92.82 ± 0.26^{ab}	-0.32 ± 0.01^{e}	4.35 ± 0.02^{c}	2.15 ± 0.23^{b}	60.3 ± 0.3^{d}	87.8 ± 0.1^{e}
Agar/ZnO	92.34 ± 0.07^{a}	-0.91 ± 0.04^{a}	6.61 ± 0.08^{d}	4.22 ± 0.09^{c}	6.76 ± 0.1^{a}	69.83 ± 0.1^{b}
Carrageenan	93.25 ± 0.42^{bc}	-0.32 ± 0.02^{d}	3.50 ± 0.09^{a}	1.35 ± 0.43^{ab}	76.04 ± 0.4^{f}	89.63 ± 0.1^{f}
Carr/ZnO	92.90 ± 0.20^{ab}	-0.58 ± 0.02^{c}	3.98 ± 0.01^{b}	1.88 ± 0.22^{ab}	19.4 ± 0.4^{c}	85.1 ± 0.1^{d}
CMC	93.44 ± 0.57^{bc}	-0.42 ± 0.01^{d}	3.40 ± 0.08^{a}	1.13 ± 0.55^{a}	61.7 ± 0.2^{e}	80.7 ± 0.1^{c}
CMC/ZnO	92.92 ± 0.17^{c}	-0.65 ± 0.02^{b}	4.16 ± 0.17^{bc}	1.34 ± 0.22^{ab}	9.1 ± 0.1^{b}	20.1 ± 0.1^{a}

Results were represented as means of replicates±standard deviation. Any two means in the same column followed by the same letter were not significantly different ($p > 0.05$) by Duncan's multiple range test.

Table 2
Thickness, moisture content, water vapor permeability, water contact angle, and tensile properties of various neat agar, carrageenan, CMC and their nanocomposite films

Films	Thickness (μm)	MC (%)	WVP ($x10^{-9}$ $g \cdot m\,m^{-2} \cdot Pa \cdot s$)	WCA (deg.)	TS (MPa)	EAB (%)	EM (MPa)
Agar	36.7 ± 5.2^{a}	18.7 ± 2.3^{a}	1.92 ± 0.12^{a}	66.5 ± 1.4^{cd}	34.6 ± 2.7^{c}	25.6 ± 2.9^{a}	1004.9 ± 88.4^{d}
Agar/ZnO	56.7 ± 5.2^{bc}	19.4 ± 0.2^{a}	1.73 ± 0.11^{a}	68.8 ± 0.2^{d}	13.0 ± 1.4^{b}	56.3 ± 7.0^{c}	109.8 ± 21.9^{bc}
Carrageenan	36.7 ± 8.2^{a}	16.8 ± 2.1^{a}	1.89 ± 0.15^{a}	61.59 ± 3.0^{c}	44.6 ± 4.7^{d}	24.2 ± 2.3^{a}	1112.1 ± 69.4^{e}
Carr/ZnO	66.7 ± 8.2^{cd}	18.2 ± 0.2^{a}	1.71 ± 0.09^{a}	84.5 ± 2.4^{e}	12.3 ± 1.6^{b}	42.1 ± 3.4^{b}	130.4 ± 30.1^{c}
CMC	45.0 ± 5.5^{b}	19.0 ± 0.4^{a}	2.23 ± 0.11^{a}	31.6 ± 2.0^{a}	6.4 ± 0.9^{a}	68.7 ± 3.1^{d}	20.5 ± 2.0^{ab}
CMC/ZnO	72.7 ± 5.1^{e}	19.7 ± 1.0^{a}	1.86 ± 0.08^{a}	55.2 ± 2.1^{b}	5.1 ± 1.1^{a}	72.9 ± 8.4^{d}	14.0 ± 4.1^{a}

Results were represented as means of replicates±standard deviation. Any two means in the same column followed by the same letter were not significantly different ($p > 0.05$) by Duncan's multiple range test.

68.8 ± 0.2, 84.5 ± 2.4, and 55.2 ± 2.1 when ZnO NPs incorporated into the biopolymer films, which was probably due to the hydrophobic nature of the nanoparticles added. The neat CMC and its nanocomposite films showed significantly lower contact angle compared with those of other films. Overall, the result of WCA indicates that the films became more hydrophobic after formation of nanocomposite with ZnO. Similarly, Nafchi et al. (2012) reported that the ZnO nanorod incorporated sago starch films had higher water contact angle than the neat starch film. They also found that the hydrophobicity of the film increased more when they added more ZnO into the film. Furthermore, Anitha et al. (2012) also found that the WCA of cellulose acetate (CA) film (47°) increased profoundly up to 124° when the CA/ZnO nanocomposites were formed. They concluded that the addition of ZnO changed the hydrophilic CA film into hydrophobic film.

3.6. Water vapor barrier property

Water vapor barrier property of the films was determined by measuring permeability of water vapor through the films. The water vapor permeability (WVP) of the agar, carrageenan, CMC and their nanocomposite films were shown in Table 2. The incorporation of ZnO NPs into the polymers clearly decreased the WVP of the biopolymer films. The increased water vapor barrier property may be attributed to the water vapor impermeable nanoparticles and the formation of tortuous path for passage of water molecules by ZnO NPs addition in the polymer matrix (Yu et al., 2009). The neat agar, carrageenan, and CMC films showed higher mean values of WVP compared with those of nanocomposite films. Among the films tested, CMC and CMC/ZnO NPs exhibited higher WVP (2.23 ± 0.11, 1.86 ± 0.08 $x10^{-9}$ $g \cdot m/m^2 \cdot Pa \cdot s$) than the other films. The WVP results indicated that the water vapor barrier property of the nanocomposite films was improved compared with that of counterpart biopolymer films, though the differences were not statistically significant ($p > 0.05$). Nafchi et al. (2012) found that the WVP of sago starch film decreased from 3.81 to 1.03×10^{-11} $g\,m^{-1}\,s^{-1}\,Pa^{-1}$ when ZnO nanorod was added into the film. This is probably due to the water vapor impermeable ZnO nanorod and the formation of tortuous pathway for diffusion of water vapor. Kim et al. (2012) also found that the incorporation of ZnO into polyurethane acrylate (PUA) decreased water vapor transfer rate (WVTR) of the PUA film from 29.0 to 27.6 $g\,m^{-2}\,day^{-1}$.

3.7. Thickness and mechanical properties

The thickness and mechanical properties of the films are shown in Table 2. The thickness of neat agar, carrageenan, and CMC films were 36.7 ± 5.2, 36.7 ± 8.2 and 45.0 ± 5.5 μm, respectively, however, the thickness of these films increased for 54.5%, 81.7%, and 59.0% after formation of nanocomposite with ZnO. Similar result was observed by Li, Xing, Li, Jiang, and Ding (2010) who reported that thickness of PVC films increased with addition of ZnO NPs.

The mechanical properties of the biopolymer films were also greatly influenced by the incorporation of ZnO NPs. Tensile strength and elastic modulus of the films were greatly reduced with addition of ZnO NPs, probably due to the weak interfacial interaction between the polymer matrix and ZnO NPs. Compared with neat agar, carrageenan, and CMC films, the nanocomposite films exhibited lower values of TS and EM (Table 2). The TS of the neat agar, carrageen, and CMC films were 34.6 ± 2.7, 44.6 ± 4.7, and 6.4 ± 0.9 MPa, respectively, but they decreased down to 13.0 ± 1.4, 12.3 ± 1.6, and 5.1 ± 1.1 MPa, which corresponds to 62.4%, 72.4%, and 20.0% of reduction, respectively. Li et al. (2009) reported that the TS and Young's modulus of the polyurethane films decreased with increasing content of ZnO NPs. On the contrary, elongation at break (EAB) of the nanocomposite films increased significantlywith addition of ZnO NPs (Table 2). This result is probably due to the presence of ZnO NPs didn't interrupt in the movement of polymer chains. The differences between TS and EAB suggest that the incorporation of ZnO NPs might be caused morphological structural changes of the polymers. Yu et al. (2009) prepared ZnO/CMC/plasticized pea starch (GPS) films. In contrast to our results, the incorporation of ZnO/CMC into GPS matrix with increasing concentration could decrease elongation of the composite films, probably due better interfacial interaction between GPS matrix and ZnO/CMC mix. The mechanical property of the film is mainly depends on the distribution and density of inter and intramolecular interactions between the polymer chains (Chambi & Grosso, 2006).

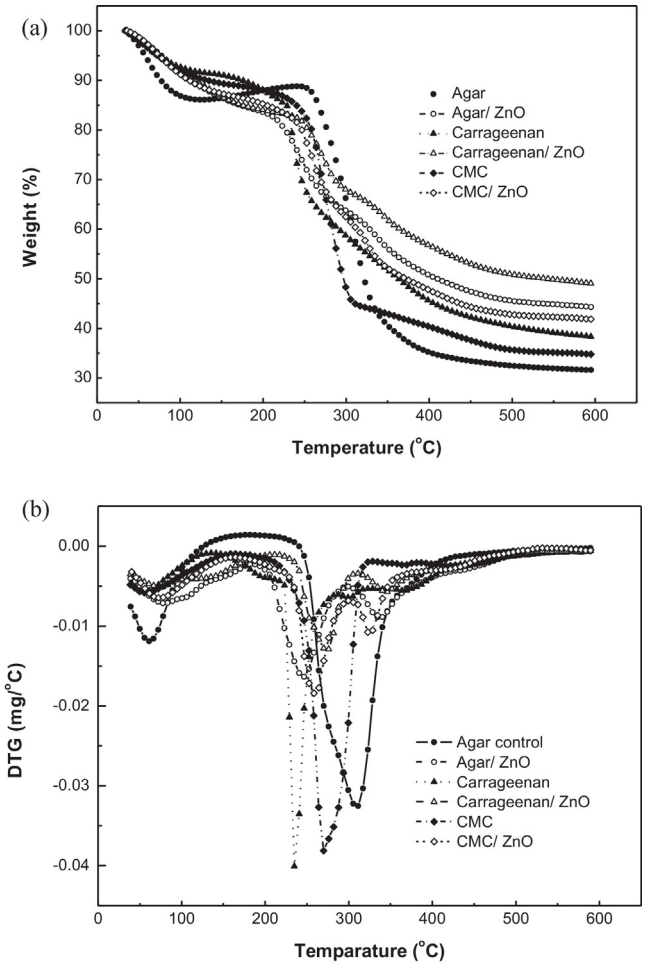

Fig. 5. TGA and Derivative form of TGA (DTGA) graph of the neat agar, carrageenan, CMC and their ZnO nanocomposite films.

3.8. Thermal property

Thermal stability of neat biopolymers and their nanocomposites films were determined by thermogravimetric analysis (TGA) and the results were shown in Fig. 5. The TGA thermograms and DTGA curves indicate clearly the weight decreasing patterns (%) and the maximum temperature (T_{max}) for the thermal decomposition of the films, respectively. As can be seen in Fig. 5a, the neat agar, carrageenan, CMC, and their nancomposite films were degraded in three steps during the thermal destruction. The first thermal degradation started at 90 °C for all the films and subsequent steps were varied depending on the film types. For example, the second and the third steps of degradation were observed at 250 °C and 325 °C for neat agar films, and they were observed at 225 °C and 330 °C for agar/ZnO NPs nanocomposite film. Carrageenan film showed second and third steps of degradation at 236 °C and 305 °C. These temperatures were observed at 233 °C and 331 °C when ZnO NPs incorporated into the carrageenan film. The first and second steps of thermal degradations were due to the evaporation of moisture and degradation of glycerol in the polymer films, respectively, and the third step of degradation was attributed to the decomposition of polymer (Rhim et al., 2006). The onset temperatures for the third step of the thermal destruction of all nanocomposite films were higher than those of neat films. These results indicate that the incorporation of ZnO NPs increased thermal stability of the polymer films. Similarly, Kim et al. (2012) reported that the thermal stability of polymer films can be improved by addition of ZnO NPs.

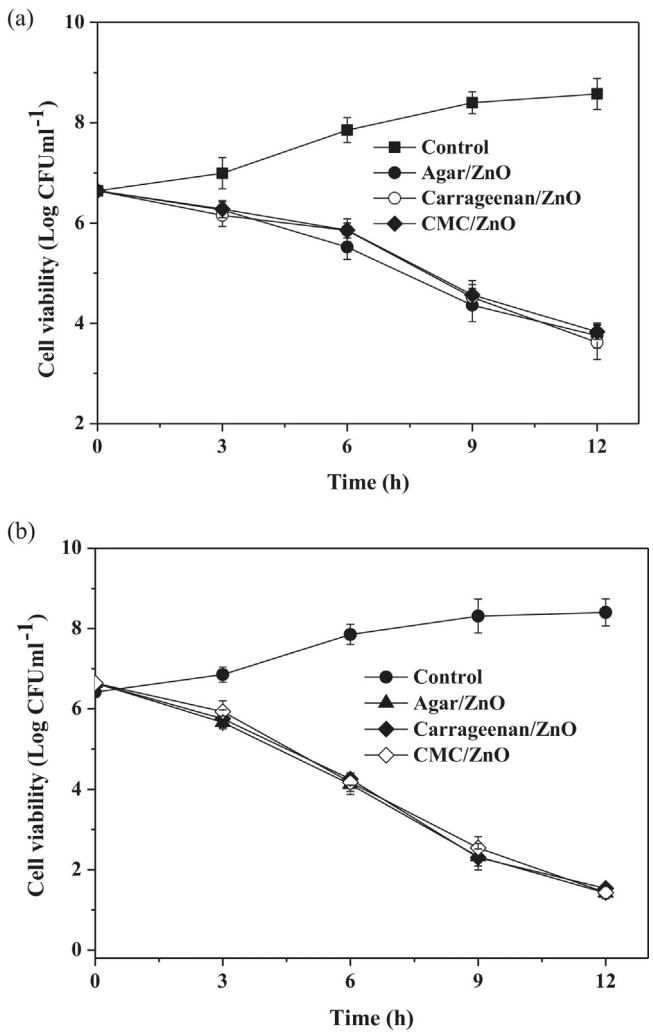

Fig. 6. Antimicrobial activity of the various nanocomposite films against (a) *E. coli* and (b) *L. monocytogenes*. The values are represented as mean ± S.D.

3.9. Antimicrobial activity

Antimicrobial activity of the films was tested against two selected food borne pathogens using a total viable cell count method. As shown in Fig. 6, neat films didn't show any antibacterial activity, however, ZnO NPs incorporated nanocomposite films showed great reduction in cell viability of both *E. coli* and *L. monocytogenes*. The agar/ZnO NPs and carrageenan/ZnO NPs films exhibited more pronounced effects than the CMC/ZnO NPs nanocomposite film. More remarkable reduction in cell viability was observed against Gram-positive *L. monocytogenes* than Gram-negative *E. coli*. These results indicated that ZnO NPs were more effective against Gram-positive than the Gram-negative bacterium. Anitha et al. (2012) also reported that ZnO NPs incorporated CA films exhibited stronger antimicrobial activity against Gram-positive than against Gram negative bacteria. They found that Gram-positive *Staphylococcus aureus* was more highly suppressed by ZnO NPs than the Gram-negative *E. coli*, *Citrobacter freundii,* and *Klebsiella pneumonia*. Nafchi et al. (2012) also studied the antimicrobial activity of sago starch/ZnO nanocomposite films. The ZnO incorporated sago starch film was more active against *S. aureus* than the *E. coli*. It is believed that antimicrobial activity of ZnO is mainly depends on the cell wall structure of the Gram-positive and Gram-negative bacteria. The Gram-positive bacteria are composed of thick cell wall structure with multilayers of

peptidoglycan, while the Gram-negative bacteria are composed of complex cell wall structure with thin peptidoglycan layer surrounded by outer membrane (Paisoonsin et al., 2013; Anitha et al., 2012). The presence of ZnO NPs are directly bind with outer cell wall of Gram-positive bacteria which contains plenty of pores to make easy penetration of nanoparticles into the cells and thus causing leakage of intracellular contents and leads to cell death (Xiao-fang et al., 2010). But in the case of Gram-negative bacteria, the ZnO NPs bind initially with bacterial outer cell membrane which contains lipoprotein, lipopolysaccharide and phospholipids that may reduce the attachment of ZnO NPs (Anitha et al., 2012). Furthermore, several possible mechanistic actions for antimicrobial activity of ZnO NPs have been proposed. First one is regarding the generation of highly reactive oxygen species (ROS) such as hydrogen peroxide, peroxide ions, hydroxyl and superoxide radicals, and singlet oxygen from the surface of ZnO NPs (Li et al., 2009; Tankhiwale, & Bajpai, 2012; Paisoonsin et al., 2013). The negatively charged superoxide and hydroxyl radicals will stay in outer cell wall membrane of bacteria and can damage the proteins, lipids and DNA, while hydrogen peroxide can penetrate into the cell wall membrane of bacteria and leads to cell death (Tankhiwale & Bajpai, 2012; Paisoonsin et al., 2013). In addition, Zhang et al. (2010) studied the mechanistic actions of ZnO NPs against *E. coli* and reported that physical and chemical interactions between the ZnO NPs and biological materials played crucial role in the antibacterial activity of ZnO NPs.

4. Conclusion

The ZnO NPs were incorporated into the various biopolymers to develop antimicrobial nanocomposite films for active packaging. The solution casting method was used to prepare films and resulting films were characterized physically and mechanically. Significant changes in color, UV and visible light barrier, moisture content, water vapor permeability, water contact angle and mechanical properties were observed. Methods such as FE-SEM, FT-IR, XRD, and TGA were also performed to characterize morphological properties of the resulting nanocomposite films. Noticeable surface morphological differences were observed between the control and nanocomposite films which analyzed by FE-SEM. The ZnO NPs were evenly distributed on surface of the nanocomposite films. XRD analysis confirmed the presence of crystal zinc oxide by revealing five characteristic diffraction peaks at theta region. Thermal stability of various biopolymers was slightly influenced by the presence of ZnO NPs. The incorporation of ZnO NPs into biopolymer film possessed bacteriostatic effect which inhibited growth of various Gram-negative and Gram-positive foodborne pathogens. Time dependent reduction in cell viability was observed. This is probably due to the migration of nanoparticles incorporated into the polymeric films. The used biopolymers may be physically entrapped nanoparticles and released by replacing with water molecules to exhibit antimicrobial effect. Based on the above experimental results, biopolymer based nanocomposite films had potential to be used as environment friendly antimicrobial packaging films to improve shelf life of food and can be used as promising alternative to synthetic or petroleum based packaging films. Nevertheless, further studies are needed to analyze their potential performance in improvement of real food stuffs.

Acknowledgements

This research was supported by the iPET (Korea Institute of Planning and Evaluation for Technology in Food, Agriculture, Forestry and Fisheries), Ministry for Food, Agriculture, Forestry and Fisheries, Republic of Korea.

References

Almasi, H., Ghanbarzadeh, B., & Entezami, A. A. (2010). Physicochemical properties of starch – CMC – nanoclay biodegradable films. *International Journal of Biological Macromolecules*, *46*, 1–5.

Anitha, S., Brabu, B., John Thiruvadigal, D., Gopalakrishnan, C., & Natarajan, T. S. (2012). Optical, bactericidal and water repellent properties of electrospun nanocomposite membranes of cellulose acetate and ZnO. *Carbohydrate Polymer*, *87*, 1065–1072.

Chambi, H., & Grosso, C. (2006). Edible films produced with gelatin and casein cross-linked with transglutaminase. *Food Research International*, *39*, 458–466.

Espitia, P. J. P., Soares, N. F. F., Teófilo, R. F., Coimbra, J. S. R., Vitor, D. M., Batista, R. A., Ferreira, S. O., Andrade, N. J., & Medeiros, E. A. A. (2013). Physical-mechanical and antimicrobial properties of nanocomposite films with pediocin and ZnO nanoparticles. *Carbohydrate Polymer*, *94*, 199–208.

FDA, Part 182-Substances generally recognized as safe. (2011) Retrieved from . 13 (2011);9http://ecfr.gpoaccess.gov/cgi/t/text/text-idx?c=ecfr&sid=786-bafc6f6343634fbfs79fcdca7061e1&rgn=div5&view=text&node=21:3.0.1.1.13&idno=21#21:3.0.1.1 Accessed 13.09.13.

Gennadios, A., Weller, C. L., & Gooding, C. H. (1994). Measurement errors in water vapor permeability of high permeable, hydrophilic edible films. *Journal of Food Engineering*, *21*, 395–409.

Gimenez, B., Lopez de Lacey, A., Perez-Santín, E., Lopez-Caballero, M. E., & Montero, P. (2013). Release of active compounds from agar and agar-gelatin films with green tea extract. *Food Hydrocolloids*, *30*, 264–271.

Kanmani, P., & Lim, S. T. (2013). Development and characterization of novel probiotic residing pullulan/starch edible films. *Food Chemistry*, *141*, 1041–1049.

Kanmani, P., & Rhim, J. W. (2014). Physical, mechanical and antimicrobial properties of gelatin based active nanocomposite films containing AgNPs and nanoclay. *Food Hydrocolloids*, *35*, 652–664.

Kim, D., Jeon, K., Lee, Y., Seo, J., Seo, K., Han, H., & Khan, S. B. (2012). Preparation and characterization of UV-cured polyurethane acrylate/ZnO nanocomposite films based on surface modified ZnO. *Progress in Organic Coating*, *74*, 435–442.

Kurian, M., Dasgupta, A., Galvin, M. E., Ziegler, C. R., & Beyer, F. L. (2006). A novel route to inducing disorder in model polymer-layered silicate nanocomposites. *Macromolecules*, *39*(5), 1864–1871.

Li, D., & Haneda, H. (2003). Morphologies of zinc oxide particles and their effects on photocatalysis. *Chemosphere*, *51*, 129–137.

Li, J. H., Hong, R. Y., Li, M. Y., Li, H. Z., Zheng, Y., & Ding, J. (2009). Effects of ZnO nanoparticles on the mechanical and antibacterial properties of polyurethane coatings. *Progress in Organic Coating*, *64*(4), 504–509.

Li, X., Xing, Y., Li, W., Jiang, Y., & Ding, Y. (2010). Antibacterial and physical properties of poly(vinyl chloride)-based film coated with ZnO nanoparticles. *Food Science and Technology International*, *16*(3), 225–232.

Llorens, A., Lloret, E., Picouet, P. A., Trbojevich, R., & Fernandez, A. (2012). Metallic-based micro and nanocomposites in food contact materials and active food packaging. *Trends in Food Science and Technology*, *24*, 19–29.

Nafchi, A. M., Alias, A. K., Mahmud, S., & Robal, M. (2012). Antimicrobial, rheological, and physicochemical properties of sago starch films filled with nanorod-rich zinc oxide. *Journal of Food Engineering*, *113*, 511–519.

Paisoonsin, S., Pornsunthorntawee, O., & Rujiravani, R. (2013). Preparation and characterization of ZnO-deposited DBD plasma-treated PP packaging film with antibacterial activities. *Applied Surface Science*, *273*, 824–835.

Rhim, J. W. (2011). Effect of clay contents on mechanical and water vapor barrier properties of agar-based nanocomposite films. *Carbohydrate Polymer*, *86*, 691–699.

Rhim, J. W., & Ng (2007). Natural biopolymer-based nanocomposite films for packaging applications. *Critical Reviews in Food Science and Nutrition*, *47*, 411–433.

Rhim, J. W., Hong, S. I., Park, H. M., & Ng, P. K. W. (2006). Preparation and characterization of chitosan-based nanocomposite films with antimicrobial activity. *Journal of Agricultural and Food Chemistry*, *54*, 5814–5822.

Rhim, J. W., Wang, L. F., & Hong, S. I. (2013). Preparation and characterization of agar/silver nanoparticles composite films with antimicrobial activity. *Food Hydrocolloids*, *33*, 327–335.

Rosca, C., Popa, M. I., & Lisa, G. (2005). Interaction of chitosan with natural or synthetic anionic polyelectrolytes. 1. The chitosan-carboxymethyl cellulose complex. *Carbohydrate Polymer*, *62*, 35–41.

Salmieri, S., & Lacroix, M. (2006). Physicochemical properties of alginate/polycaprolactone based films containing essential oils. *Journal of Agricultural and Food Chemistry*, *54*, 10205–10214.

Sharon, M., Choudhary, A. K., & Kumar, R. (2010). Nanotechnology in agricultural diseases and food safety. *Journal of Phytology*, *2*(4), 83–92.

Shojaee-Aliabadi, S., Hosseini, H., Mohammadifar, M. A., Mohammadi, A., Ghasemlou, M., Ojagh, S. M., Hosseini, S. M., & Khaksar, R. (2013). Characterization of antioxidant antimicrobial κ-carrageenan films containing Satureja hortensis essential oil. *International Journal of Biological Macromolecules*, *52*(1), 116–124.

Soares, N. F. F., Pires, A. C. S., Camilloto, G. P., Santiago-Silva, P., Espitia, P. J. P., & Silva, W. A. (2009). Recent patents on active packaging for food application. *Recent Patents on Food, Nutrition & Agriculture*, *1*(1), 171–178.

Soradech, S., Nunthanid, J., Limmatvapirat, S., & Luangtana-anan, M. (2012). An approach for the enhancement of the mechanical properties and film coating efficiency of shellac by the formation of composite films based on shellac and gelatin. *Journal of Food Engineering*, *108*, 94–102.

Srinivasa, P. C., Ramesh, M. N., Kumar, K. R., & Tharanathan, R. N. (2003). Properties and sorption studies of chitosan–. *Carbohydrate Polymer*, *53*(4), 431–438.

Tankhiwale, R., & Bajpai, S. K. (2012). Preparation, characterization and antibacterial applications of ZnO-nanoparticles coated polyethylene films for food packaging. *Colloids and Surfaces B: Biointerfaces*, *90*, 16–20.

Tharanathan, R. N. (2003). Biodegradable films and composite coatings: Past, present and future. *Trends in Food Science and Technology*, *14*, 71–78.

Tunç, S., & Duman, O. (2011). Preparation of active antimicrobial methyl cellulose/carvacrol/montmorillonite nanocomposite films and investigation of carvacrol release. *LWT-Food Science and Technology*, *44*(2), 465–472.

Volery, P., Besson, R., & Schaffer-lequart, C. (2004). Characterization of commercial carrageenans by Fourier transform infrared spectroscopy using single-reflection attenuated total reflection. *Journal of Agricultural and Food Chemistry*, *52*, 7457–7463.

Wu, Y., Geng, F., Chang, P. R., Yu, J., & Ma, X. (2009). Effect of agar on the microstructure and performance of potato starch film. *Carbohydrate Polymer*, *76*, 299–304.

Xiao-fang, L., Xiao-qiang, F., Sheng, Y., Guo-qing, F., Ting-pu, W., & Zhong-xing, S. (2010). Chitosan kills *Escherichia coli* through damage to be of cell membrane mechanism. *Carbohydrate Polymer*, *79*, 493–499.

Yoksan, R., & Chirachanchai, S. (2010). Silver nanoparticle-loaded chitosan–starch based films: Fabrication and evaluation of tensile, barrier and antimicrobial properties. *Materials Science and Engineering C*, *30*, 891–897.

Yu, J., Yang, J., Liu, B., & Ma, X. (2009). Preparation and characterization of glycerol plasticized-pea starch/ZnO-carboxymethyl cellulose sodium nanocomposites. *Bioresource Technology*, *100*(11), 284–2832.

Zhang, L., Jiang, Y., Ding, Y., Daskalakis, N., Jeuken, L., Povey, M., O'Neill, A., & York, D. (2010). Mechanistic investigation into antibacterial behavior of suspensions of ZnO nanoparticles against *E. coli*. *Journal of Nanoparticle Research*, *12*(5), 1625–1636.